

Probing Spin-2 Ultralight Dark Matter with Space-based Gravitational Wave Detectors in Millihertz

Jing-Rui Zhang^{1,5,6,*}, Ju Chen^{2,6,†}, Heng-Sen Jiao^{3,7}, Rong-Gen Cai^{4,1,5}, and Yun-Long Zhang^{3,1,‡}

¹*School of Fundamental Physics and Mathematical Sciences,*

Hangzhou Institute for Advanced Study, UCAS, Hangzhou 310024, China.

²*International Center for Theoretical Physics Asia-Pacific (ICTP-AP),
University of Chinese Academy of Sciences, Beijing 100190, China*

³*National Astronomical Observatories, Chinese Academy of Sciences, Beijing, 100101, China*

⁴*Institute of Fundamental Physics and Quantum Technology, Ningbo University, Ningbo 315211, China*

⁵*Institute of Theoretical Physics, Chinese Academy of Sciences, Beijing 100190, China*

⁶*Taiji Laboratory for Gravitational Wave Universe (Beijing/Hangzhou),
University of Chinese Academy of Sciences, Beijing 100049, China and*

⁷*School of Astronomy and Space Science, University of Chinese Academy of Sciences, Beijing 100049, China*

Spin-2 ultralight dark matter (ULDM) is a viable dark matter candidate and it can be constrained using gravitational wave (GW) observations. In this paper, we investigate the detectability of spin-2 ULDM by space-based GW interferometers. By considering a direct coupling between spin-2 ULDM and ordinary matter, we derive the corresponding response functions and sensitivity curves for various time-delay interferometry channels and calculate the optimal sensitivity curves for future millihertz GW detectors. Our results demonstrate that the space-based detectors can place stringent constraints on the coupling constant of spin-2 ULDM, reaching $\alpha \sim 10^{-10}$ around a mass of $m \sim 10^{-17}$ eV, surpassing current limits from ground-based detectors and pulsar timing arrays. Thus, the space-based GW detectors can serve as powerful tools not only for detecting GWs but also for probing fundamental properties of ultralight dark matter.

CONTENTS

I. Introduction	1
II. Spin-2 ULDM	2
III. Response function for spin-2 ULDM	2
A. Single link	2
B. Michelson configuration	4
C. Michelson TDI combinations	4
IV. Constraints on spin-2 ULDM	5
A. Sensitivity curves of space-based GWIs	5
B. Constraints on spin-2 ULDM	5
V. Conclusion	7
Acknowledgments	8
A. Sagnac TDI combinations	8
1. Sagnac combinations	8
2. Fully symmetric Sagnac combination	9
B. AET channels	9
References	10

I. INTRODUCTION

In recent years, gravitational waves (GWs) are getting increasing attention at the frontier of both theoretical and experimental physics. Ground-based gravitational wave interferometers (GWIs) have achieved notable success in the detection of GWs, including the first discovery in 2015 [1], and the observation of GWs accompanied by electromagnetic counterparts in 2017 [2]. More recently, several pulsar timing array (PTA) collaborations reported evidence for the detection of a nanohertz stochastic GW background [3–6]. Also, direct and indirect methods are being used to capture evidence of primordial GWs [7–9]. The study of GWs has become a thriving field, offering a wealth of phenomena for physics and astronomy.

Apart from detecting GWs, GWIs can also be utilized to detect dark matter [10–13], particularly ultralight dark matter (ULDM). ULDM refers to ultralight bosonic particles with masses $m \lesssim 1$ eV. These particles have been extensively studied recently, as potential solutions to the problems of the cold dark matter model at small scale [14, 15]. The oscillation of ULDM could produce signals detectable by GWIs if ULDM interacts with GWIs, such as through coupling to the test masses or laser photons. This makes it possible to directly probe ULDM with GWIs when its oscillation frequency, falls within the sensitivity range of GWIs. On the other hand, if ULDM exists around black holes, it could have non-negligible effects, such as influencing binary black hole dynamics [16–18] or inducing superradiance [19, 20]. These effects suggest that GWIs can also be used for indirect ULDM searches [21–25]. Recently,

* zhangjingrui22@mails.ucas.ac.cn

† chenju@ucas.ac.cn

‡ zhangyunlong@nao.cas.cn

the prospects of detecting ULDM with GWs have been widely studied [26–39], and constraints based on the observation from current GWs have also been placed on various types of ULDM [40–52].

Depending on its spin, ULDM can be classified into different species, including spin-0, spin-1, and spin-2 particles. Considerable efforts have been made to study spin-0 and spin-1 ULDM, leading to notable constraints on their parameter space [40–42, 44, 45, 53]. For spin-2 ULDM, the research on ground-based GWs [25, 31, 49] and PTAs [54–57] has been focused. The detailed investigations of spin-2 ULDM using space-based GWs remain lacking.

Recently, space-based GWs [58–60] have gained increasing interest in GW astronomy. A space-based GWI consists of three separate spacecrafts, forming an approximate equilateral triangle in space. Each spacecraft acts both as a laser signal transmitter and receiver, measuring the separation between free-falling test masses inside each spacecraft. Relative changes in the separation are analyzed to determine if they originate from the effects of GWs. The data stream is processed using the time-delay interferometry (TDI) algorithm [61], which helps eliminate major sources of noise in space-based GWIs, such as laser frequency noise and clock noise. Several space-based GWI projects have been proposed, including LISA [58], Taiji [59], and TianQin [60]. In the future, these projects will not only provide valuable information about GWs in the millihertz band, but will also serve as detectors for searches of ULDM.

In this paper, we demonstrate the potential of space-based GWIs for detecting spin-2 ULDM. Spin-2 ULDM typically has two possible interactions with GWs: direct coupling with standard model particles and its gravitational effect. Here, we focus on its direct coupling with ordinary matter. For its gravitational effect, one can refer to [39, 57]. The paper is organized as follows. In Section II, we revisit the basics of spin-2 ULDM. In Section III, the responses of space-based GWIs to spin-2 ULDM in different TDI combinations are calculated and compared. In Section IV, possible constraints from space-based GWIs on spin-2 ULDM are presented. In Section V, we conclude and discuss the results. Throughout the paper, we use the convention $\hbar = c = 1$.

II. SPIN-2 ULDM

The idea of spin-2 dark matter dates back to 2004 [62], when the massive graviton was considered as a dark matter candidate. After the bimetric theory was introduced in [63], this idea was revitalized, with explorations of its viability as a dark matter candidate across various mass ranges [64–68]. More recently, spin-2 dark matter with ultralight mass was found to be detectable with GW detectors [31, 54, 55, 57, 69, 70]. In this work, we examine the detectability of spin-2 ULDM using space-based GWIs.

For spin-2 ULDM, its effects on space-based GWIs are similar to those of GWs. Therefore, the treatment for GWs [71, 72] can be adapted to account for the effects of spin-2 ULDM. The occupation number of spin-2 ULDM is as large as $\frac{\rho_{\text{DM}}}{m \cdot (mv)^3} \approx 10^{71} \left(\frac{\rho_{\text{DM}}}{0.4 \text{ GeV/cm}^3} \right) \left(\frac{10^{-17} \text{ eV}}{m} \right)^4 \left(\frac{10^{-3}}{v} \right)^3$, which makes it reasonable for us to treat it as a classical field. Considering the spin-2 ULDM as a plane wave, its field component can be described as

$$M_{ij}(t, \vec{x}) = \frac{\sqrt{2\rho_{\text{DM}}}}{m} \varepsilon_{ij} e^{i(mt - m\vec{v}\cdot\vec{x})}, \quad (1)$$

where ρ_{DM} is the energy density of dark matter around the solar system, approximately 0.4 GeV/cm^3 . m is the mass of spin-2 ULDM, and \vec{v} is the velocity of the spin-2 ULDM, with a typical value in the solar system of $\sim 10^{-3}$, allowing us to safely approximate the energy of spin-2 ULDM as its mass. ε represents the polarization tensor. Components $M_{0\nu}$ are suppressed by $v/c \sim 10^{-3}$ and can be ignored. Unlike GWs, spin-2 ULDM has 5 independent polarization modes:

$$\begin{aligned} \varepsilon_{ij}^{\times} &= \frac{1}{\sqrt{2}}(p_i q_j + q_i p_j), \quad \varepsilon_{ij}^{\dagger} = \frac{1}{\sqrt{2}}(p_i p_j - q_i q_j), \\ \varepsilon_{ij}^{\text{L}} &= \frac{1}{\sqrt{2}}(q_i r_j + r_i q_j), \quad \varepsilon_{ij}^{\text{R}} = \frac{1}{\sqrt{2}}(p_i r_j + r_i p_j), \\ \varepsilon_{ij}^{\text{S}} &= \frac{1}{\sqrt{6}}(3r_i r_j - \delta_{ij}), \end{aligned} \quad (2)$$

where \hat{r} is the unit vector in the reference direction for polarization decomposition, \hat{p} and \hat{q} are two unit vectors perpendicular to \hat{r} and to each other. Note that these polarization tensors are normalized such that $\varepsilon_{ij}^A \varepsilon^{A',ij} = \delta^{AA'}$, which differs from the usual conventions for GWs.

III. RESPONSE FUNCTION FOR SPIN-2 ULDM

The spin-2 ULDM couples to matter universally with a factor $\frac{\alpha}{M_{\text{Pl}}}$, such that we can evaluate its effect by changing the frame to $\tilde{g}_{\mu\nu} = g_{\mu\nu} - \frac{\alpha}{M_{\text{Pl}}} M_{\mu\nu}$. Since $m \gg H$, we can ignore the Hubble constant and work with $\tilde{g}_{ij} = \delta_{ij} - \frac{\alpha}{M_{\text{Pl}}} M_{ij}$. Note that this form of the metric fluctuations resembles the synchronous gauge in the treatment for GWs, in which $h_{00} = h_{0i} = 0$. Therefore, when we evaluate the effect of spin-2 ULDM on GWIs, we can focus on the Shapiro effect on photons [73], which causes a frequency shift of the photon. In this section, we calculate the response of spin-2 ULDM with space-based GWIs following a treatment similar to that of GWs.

A. Single link

We first evaluate the effect of spin-2 ULDM for a single link, in which the photon simply travels from one test

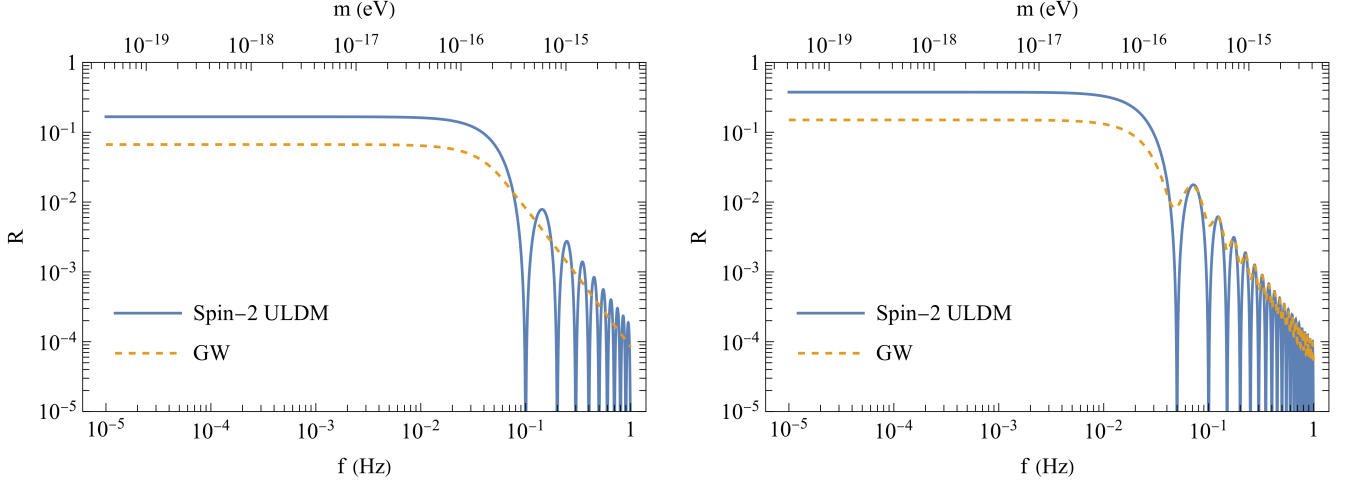


FIG. 1. The response functions for single link(left) and Michelson combinations(right).

mass to another one. For a photon with 4-momentum $p^\mu = \nu(1, -\hat{n}_{rs}^i)$, where \hat{n}_{rs}^i is the unit vector pointing from the receiver r to the sender s , the geodesic equation gives

$$\frac{dp^0}{du} = \frac{\alpha\nu^2}{2M_{\text{Pl}}} \partial_t M_{ij} n_a^i n_a^j, \quad (3)$$

where u is the affine parameter. After a similar treatment with GWs, we can obtain the frequency shift of the photon

$$z_{rs}(t) = \frac{\Delta\nu}{\nu_o} = -\frac{\alpha}{2M_{\text{Pl}}(1 + \vec{v} \cdot \hat{n}_{rs})} \hat{n}_{rs}^i \hat{n}_{rs}^j \times [M_{ij}(t_r, \vec{x}_r) - M_{ij}(t_s, \vec{x}_s)], \quad (4)$$

where ν_o is the original frequency of the photon. Note that in the denominator, the factor is $(1 + \vec{v} \cdot \hat{n}_{rs})$, which is different from GWs [74], where the factor is $(1 + \hat{n} \cdot \hat{n}_{rs})$, in which \hat{n} represents the direction of GWs. This is because the speed of spin-2 ULDM cannot reach the speed of light and is typically far from it. Here we adapt the usual treatment that $v/c \approx 10^{-3}$.

The frequency shift can be transformed into the change of arm length

$$s(t) = \frac{\Delta L}{L} = \frac{\ell_{rs} - L}{L} = \frac{\Delta\Phi_{rs}}{\nu L} = \frac{\int_0^t z_{rs} dt}{L} \quad (5)$$

$$= -\frac{\alpha \hat{n}_{rs}^i \hat{n}_{rs}^j [M_{ij}(t + L, \vec{x}_r) - M_{ij}(t, \vec{x}_s)]}{2iM_{\text{Pl}}mL(1 + \vec{v} \cdot \hat{n}_{rs})}, \quad (6)$$

where ℓ_{rs} is the perturbed arm length and L is the nominal arm length of the detector. Following the notation used in treatments of GWs [71], we can view Eq. (6) as the contraction between the detector tensor D^{ij} and the signal h_{ij}

$$s(t) = D^{ij}(\vec{v}) h_{ij}(t, \vec{x}_s), \quad (7)$$

where

$$D^{ij}(\vec{v}) = \frac{1}{2} \mathcal{T}(\vec{v} \cdot \hat{n}_{rs}) \hat{n}_{rs}^i \hat{n}_{rs}^j, \quad (8)$$

$$h_{ij}(t, \vec{x}_s) = -h_M \varepsilon_{ij} e^{i(mt - m\vec{v} \cdot \vec{x}_s)}. \quad (9)$$

Here,

$$h_M = \frac{\alpha\sqrt{2\rho_{\text{DM}}}}{mM_{\text{Pl}}}, \quad (10)$$

and \mathcal{T} is the transfer function

$$\mathcal{T}(\vec{v} \cdot \hat{n}_{rs}) = \text{sinc}[\phi_m(1 + \vec{v} \cdot \hat{n}_{rs})] e^{i\phi_m(1 + \vec{v} \cdot \hat{n}_{rs})}, \quad (11)$$

where $\text{sinc } x \equiv \frac{\sin x}{x}$, and we have introduced $\phi_m \equiv \frac{mL}{2}$. The antenna pattern function $F^A(\vec{v})$ is defined as the contraction between the detector tensor D^{ij} and the polarization tensor ε_{ij}

$$F^A(\vec{v}) = D^{ij}(\vec{v}) \varepsilon_{ij}^A, \quad (12)$$

and the response function is

$$\mathcal{R} = \int \frac{d^2\hat{v}}{4\pi} \int \frac{d^2\hat{r}}{4\pi} \sum_A F^{A*}(\vec{v}) F^A(\vec{v}), \quad (13)$$

where $\int d^2\hat{r}/4\pi$ represents averaging over the directions of polarizations over the sky.

For the single link, the response function can be analytically obtained as

$$\mathcal{R} = \frac{1-v}{12v} \text{sinc}^2[\phi_m(1-v)] - \frac{1+v}{12v} \text{sinc}^2[\phi_m(1+v)] - \frac{\text{Si}[2\phi_m(1-v)]}{12v\phi_m} + \frac{\text{Si}[2\phi_m(1+v)]}{12v\phi_m}, \quad (14)$$

where $\text{Si } x \equiv \int_0^x \frac{\sin t}{t} dt$, and numerical values are calculated and shown in Fig. 1. In the calculation, we assume

the detector arm length to be $L = 3 \times 10^9$ m and adopt $v = 10^{-3}$, which is a typical value for the velocity of dark matter localized in the solar system. Note that the responses are expressed as functions of the mass m , and for comparison with GWs, we also present the corresponding frequency in the plot, given by $m = 2\pi f$.

From the figure, we observe that for spin-2 ULDM, the response function exhibits frequent drops at higher frequencies, near integer multiples of $\frac{1}{L}$. In contrast, the response curve for GWs remains smooth, without such drops. Expanding Eq. (14) around these drops, we find that the response function \mathcal{R} becomes $\frac{v^2}{18} + \mathcal{O}(v^3)$, with the frequency given by $f = N(\frac{1}{L} + \frac{2v^2}{3L}) + \mathcal{O}(v^3)$, where N is a positive integer. These drops arise from the limited velocity of spin-2 ULDM. In particular, if we assume the speed of spin-2 ULDM to be zero, the response function becomes $\mathcal{R} = \text{sinc}^2(mL/2)/6$, which equals zero at $f = \frac{N}{L}$.

B. Michelson configuration

For a normal equal-arm Michelson configuration, the signal can be expressed as:

$$s_{\text{m1}}(t) = \frac{1}{2L} [\ell_{21}(t-2L) + \ell_{12}(t-L) - \ell_{31}(t-2L) - \ell_{13}(t-L)], \quad (15)$$

where $\ell_{rs} = L[1 + s(t)]$, as given in Eq.(6). Similarly, we can introduce the detector tensor of $D_{\text{m1}}^{ij}(\vec{v})$, and:

$$s_{\text{m1}}(t) = D_{\text{m1}}^{ij}(\vec{v})h_{ij}(t, \vec{x}_1). \quad (16)$$

With Eqs. (6) and (9), we obtain

$$D_{\text{m1}}^{ij}(\vec{v}) = \frac{1}{2} [n_{21}^i n_{21}^j \mathcal{T}_{\text{m1}}(\vec{v} \cdot \hat{n}_{21}) - n_{31}^i n_{31}^j \mathcal{T}_{\text{m1}}(\vec{v} \cdot \hat{n}_{31})], \quad (17)$$

and the transfer function

$$\mathcal{T}_{\text{m1}}(\vec{v} \cdot \hat{n}_{rs}) = \frac{1}{2} [\text{sinc}(\phi_m(1 + \vec{v} \cdot \hat{n}_{rs})) e^{i\phi_m(-3 + \vec{v} \cdot \hat{n}_{rs})} + \text{sinc}(\phi_m(1 - \vec{v} \cdot \hat{n}_{rs})) e^{i\phi_m(-1 + \vec{v} \cdot \hat{n}_{rs})}]. \quad (18)$$

The response function can then be evaluated using Eqs. (12) and (13), and the result is shown in Fig. 1. From the figure, we can see that the general behavior of spin-2 ULDM resembles GWs, with two main differences. Firstly, the low-frequency limit of the response function is 0.375, which is $\frac{5}{2}$ times that of GWs. This is again due to the greater freedom of polarization states in spin-2 ULDM. Note that we use the normalization convention $\varepsilon_{ij}^A \varepsilon^{A',ij} = \delta^{AA'}$, so the value here is half of the value found in some other literature [74]. Secondly, the drop at high frequencies is more pronounced for spin-2 ULDM compared to GWs, due to the relatively slow speed of spin-2 ULDM, as analyzed in Sec. III A.

C. Michelson TDI combinations

For space-based GWIs, the distances between different arms cannot be strictly fixed to be equal. As a result, laser frequency noise becomes dominant and can far exceed GW signals. To address this problem, time-delay interferometry (TDI) was introduced, enabling virtual equal-arm interference through a linear combination of time-shifted signals [61]. We calculate and compare the response of common TDI channels. Since the final sensitivity is independent of the TDI generation, provided that the laser noise is sufficiently suppressed, we consider only the first-generation TDI (or TDI 1.5) as a demonstration. For simplicity, we assume that all arm lengths are constant and equal.

Here, we present the results for the Michelson TDI configurations. The formulas for the Sagnac and AET combinations are provided in Appendix A 1 and Appendix B, respectively. For Michelson X combinations, the signal is

$$s_X(t) = \frac{1}{4L} [\ell_{21}(t-4L) + \ell_{12}(t-3L) + \ell_{31}(t-2L) + \ell_{13}(t-L) - \ell_{31}(t-4L) - \ell_{13}(t-3L) - \ell_{21}(t-2L) - \ell_{12}(t-L)] \quad (19)$$

$$= D_X^{ij}(\vec{v})h_{ij}(t, \vec{x}_1). \quad (20)$$

The corresponding detector tensor is given by

$$D_X^{ij}(\vec{v}) = \frac{1}{2} [n_{21}^i n_{21}^j \mathcal{T}_{\text{mx}}(\vec{v} \cdot \hat{n}_{21}) - n_{31}^i n_{31}^j \mathcal{T}_{\text{mx}}(\vec{v} \cdot \hat{n}_{31})], \quad (21)$$

and the transfer function

$$\mathcal{T}_{\text{mx}}(\vec{v} \cdot \hat{n}_{rs}) = -\frac{1}{2}(1 - e^{-4i\phi_m})\mathcal{T}_{\text{m1}}(\vec{v} \cdot \hat{n}_{rs}). \quad (22)$$

The Michelson Y and Z combinations can be obtained by cyclic permutations of the spacecraft labels {1, 2, 3} in the expression of X. After averaging the direction of velocity, the response functions of X, Y and Z channels for spin-2 ULDM become the same, which is confirmed by our numerical calculations.

The response functions of spin-2 ULDM are shown in Fig. 2, which are compared with those of GWs. The response functions of GWs are calculated in a manner analogous to those for spin-2 ULDM, with two main differences. Firstly, the polarization tensors for GWs are restricted to “+” and “ \times ” modes. Secondly, the velocity \vec{v} and the reference vector \hat{r} for spin-2 ULDM are replaced by the directions of GWs, denoted by \hat{n} , and averaging over \hat{v} and \hat{r} is substituted by averaging over \hat{n} in Eq. (13). In the low-frequency limit, due to the different degrees of freedom for polarizations, the response function for spin-2 ULDM behaves as $\frac{3}{2}\pi^2 L^2 f^2$, while for GWs, it follows $\frac{3}{5}\pi^2 L^2 f^2$. At relatively high frequencies, both responses exhibit similar behavior. This can be understood by comparing the Michelson configuration in Sec. III B with the X channel here. The response functions of the two channels differ by a factor of $\sin^2(mL)$,

which drives the response function of GWs to zero at the drops in high frequency, making its response curve more closely resemble that of spin-2 ULDM.

IV. CONSTRAINTS ON SPIN-2 ULDM

In order to quantitatively examine the detectability of space-based GW detectors on spin-2 ULDM, we calculate the sensitivity in different TDI channels and then give the constraint on the coupling constant α for spin-2 ULDM with different mass m .

A. Sensitivity curves of space-based GWIs

The sensitivity of each TDI channel can be obtained through

$$S_h = \frac{N_h}{\mathcal{R}_h}, \quad (23)$$

where h is the label for each channel. The response functions \mathcal{R}_h for spin-2 ULDM and GWs are calculated in Sec. III. N_h denotes the one-sided noise spectral density. The remaining secondary noises after the TDI process include the Optical Metrology System (OMS) noise and the test mass acceleration (acc) noise. For LISA [58], Taiji [59] and TianQin [60], the power spectral densities of these noises are given by

$$P_{\text{OMS}} = A_{\text{OMS}}^2 \left[1 + \left(\frac{2\text{mHz}}{f} \right)^4 \right], \quad (24)$$

$$P_{\text{acc}} = A_{\text{acc}}^2 \left[1 + \left(\frac{0.4\text{mHz}}{f} \right)^2 \right] \left[1 + \left(\frac{f}{8\text{mHz}} \right)^4 \right], \quad (25)$$

where A_{OMS} , A_{acc} and arm length L for different detectors are listed in Table I. For different TDI channels, we utilize the noise spectral density derived in [37], with modification to adjust to our convention:

$$\begin{aligned} N_X &= \frac{1}{L^2} \sin^2 \frac{f}{f_*} \left[P_{\text{OMS}} + (3 + \cos \frac{2f}{f_*}) \frac{P_{\text{acc}}}{(2\pi f)^4} \right], \\ N_A = N_E &= \frac{1}{2L^2} \sin^2 \frac{f}{f_*} \left[(2 + \cos \frac{f}{f_*}) P_{\text{OMS}} \right. \\ &\quad \left. + (6 + 4 \cos \frac{f}{f_*} + 2 \cos \frac{2f}{f_*}) \frac{P_{\text{acc}}}{(2\pi f)^4} \right], \\ N_T &= \frac{2}{L^2} \sin^2 \frac{f}{2f_*} \sin^2 \frac{f}{f_*} \left[P_{\text{OMS}} + 4 \sin^2 \frac{f}{2f_*} \frac{P_{\text{acc}}}{(2\pi f)^4} \right], \\ N_\alpha &= \frac{1}{9L^2} \left[6P_{\text{OMS}} + (16 \sin^2 \frac{f}{2f_*} + 8 \sin^2 \frac{3f}{2f_*}) \frac{P_{\text{acc}}}{(2\pi f)^4} \right], \\ N_\zeta &= \frac{2}{3L^2} \left[P_{\text{OMS}} + 4 \sin^2 \frac{f}{2f_*} \frac{P_{\text{acc}}}{(2\pi f)^4} \right], \end{aligned} \quad (26)$$

where $f_* \equiv c/(2\pi L)$.

The sensitivity curves of spin-2 ULDM for different channels, along with those of GWs, are shown in Fig. 3.

	A_{OMS}	A_{acc}	L
LISA	15pm/ $\sqrt{\text{Hz}}$	3fm/s ² / $\sqrt{\text{Hz}}$	2.5Gm
Taiji	8pm/ $\sqrt{\text{Hz}}$	3fm/s ² / $\sqrt{\text{Hz}}$	3.0Gm
TianQin	1pm/ $\sqrt{\text{Hz}}$	1fm/s ² / $\sqrt{\text{Hz}}$	0.17Gm

TABLE I. Noise amplitude spectral density parameters and arm lengths for different space-based GW detectors.

The comparison between different channels is depicted in Fig. 4. As shown in the plots, the symmetric channels, including the fully symmetric Sagnac combination ζ and channel T, exhibit a much worse sensitivity to spin-2 ULDM, being three orders of magnitude higher than those of GWs. Combined with the results in [37], these channels may be good candidates to avoid the effects of ULDM on GWI during the detection of GWs. Combined with the results in [37], these channels may serve as promising candidates for mitigating the effects of ULDM on GWIs during gravitational wave detection, particularly at higher frequencies when $f \gtrsim 10\text{mHz}$, where the sensitivity of GWs in symmetric channels is comparable to that of other asymmetric TDI channels. The sensitivities of the A/E and X channels are similar at low frequencies, while at higher frequencies the A/E channels show slightly better sensitivity. For the Sagnac α channel, the sensitivity is also low at low frequencies, but at higher frequencies, it becomes comparable to that of the A channel. We also calculate the optimal sensitivity curve, which combines the sensitivities of all independent TDI channels [37, 75],

$$1/S_\eta = 1/S_A + 1/S_E + 1/S_T, \quad (27)$$

and use it to place constraints on spin-2 ULDM. The result is shown in Fig. 5, where the optimal sensitivity curves for three different space-based GWIs are presented. We can observe that LISA and Taiji exhibit better sensitivity at low frequencies, while TianQin performs better at higher frequencies due to its shorter arm length.

B. Constraints on spin-2 ULDM

For spin-2 ultralight dark matter, there are two main parameters: the mass m and the coupling constant α . The mass corresponds to the frequency of the signal that appears in the detector response. The coupling constant describes the potential nontrivial interactions between spin-2 ULDM and matter as outlined in bimetric theory [68]. Using the optimal sensitivity introduced in the previous section, we can place constraints on α for each mass of spin-2 ULDM.

We assume the spin-2 ULDM is fully virialized, so the five polarization modes are equally distributed. As the observation time T_{obs} increases, the signal would accu-

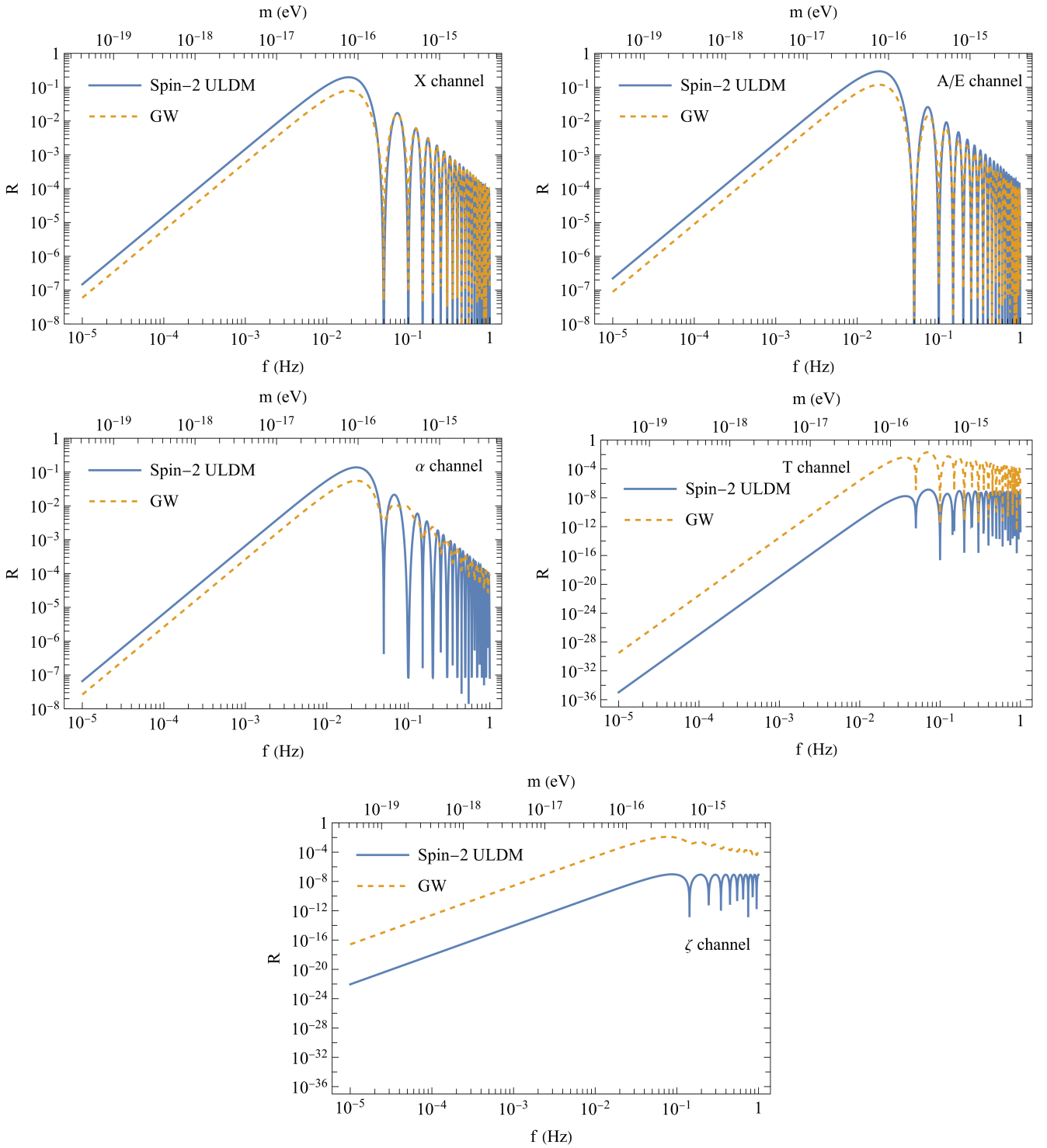


FIG. 2. The response functions for different TDI channels.

mulate as

$$\frac{h_M}{\sqrt{5}} \sqrt{T_{\text{obs}}} = \frac{\alpha \sqrt{2\rho_{\text{DM}}}}{\sqrt{5}mM_{\text{Pl}}} \sqrt{T_{\text{obs}}}, \quad (28)$$

where h_M is the amplitude of the signal h_{ij} in (10). The additional factor $\sqrt{5}$ in the denominator accounts

for summing over all polarization modes in the calculation of the response function. When the accumulated signal reaches the sensitivity of detectors $\sqrt{S_\eta}$, it can eventually be detected [37].

Here we assume the observation time is shorter than the coherence time of spin-2 ULDM $T_{\text{coh}} = 2\pi/(\frac{1}{2}mv^2) \approx$

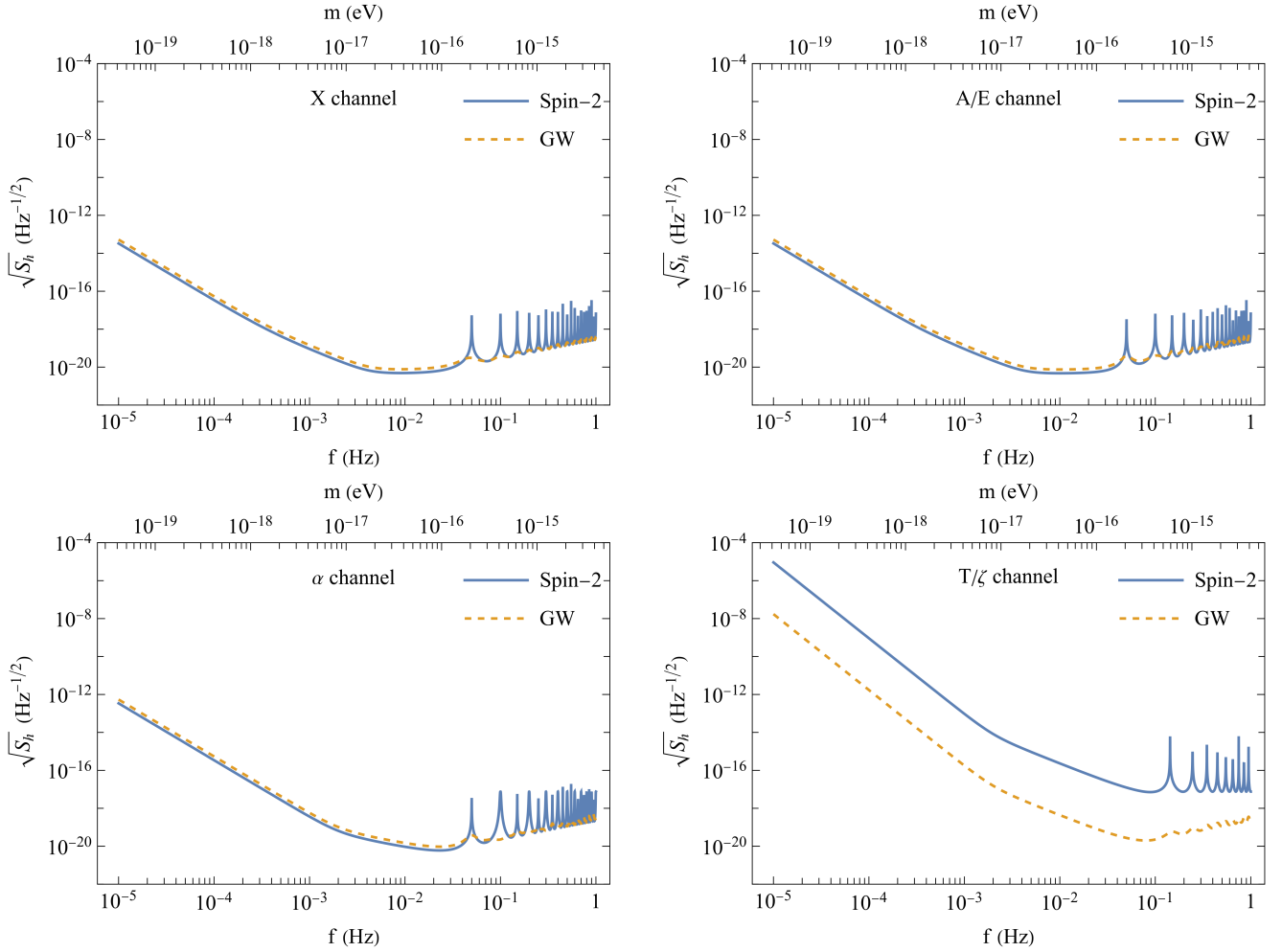


FIG. 3. The sensitivity curves of GWs for the detection of spin-2 ULDM in different TDI channels, compared with the performance of GWs. We assume $L = 3 \times 10^9$ m and $v = 10^{-3}$.

8×10^7 s $\left(\frac{10^{-16} \text{ eV}}{m}\right)$, then the approximation that spin-2 ULDM can be treated as monochromatic plane waves still holds. With this, we can get the constraint on α for different mass parameters:

$$\alpha = \frac{m M_{\text{Pl}}}{\sqrt{T_{\text{obs}}}} \sqrt{\frac{5 S_{\eta}}{2 \rho_{\text{DM}}}}. \quad (29)$$

The final constraints are shown in Fig. 6. We find that the strongest constraint on α is about 10^{-10} , achieved by Taiji at $m \approx 10^{-17}$ eV, which is a very strong limit compared to current results from ground-based GWs and PTAs. Additionally, LISA and Taiji exhibit better sensitivity at low frequencies in the search for spin-2 ULDM, while TianQin shows improved sensitivity at frequencies $f \gtrsim 0.04$ Hz. It is worth noting that if spin-2 ULDM constitutes only a fraction of the total dark matter density, the constraint is actually on $\sqrt{\rho_2/\rho_{\text{DM}}}\alpha$ instead of α , where ρ_2/ρ_{DM} represents the fraction of spin-2 ULDM in the total dark matter.

V. CONCLUSION

In this paper, we investigate the potential of space-based GWs for detecting spin-2 ULDM. We examine the effect of spin-2 ULDM on the detector, considering the direct coupling between spin-2 ULDM and ordinary matter. We calculate the corresponding response functions and sensitivity curves for various TDI channels. Our results show that future space-based GWs could place stringent constraints on the coupling constant of spin-2 ULDM, reaching 10^{-10} at $m \approx 10^{-17}$ eV, which is about two orders of magnitude stronger than current results from ground-based GWs and PTAs. It is also interesting that fully symmetric TDI channels exhibit worse sensitivity to spin-2 ULDM compared to GWs. This difference may provide an opportunity to distinguish ULDM signals from GWs when sufficient observational data are accumulated.

It is worth noting that we assume the speed of spin-2 ULDM is fixed at 10^{-3} in our calculations. In reality, the speed of virialized ULDM follows a Maxwellian distribu-

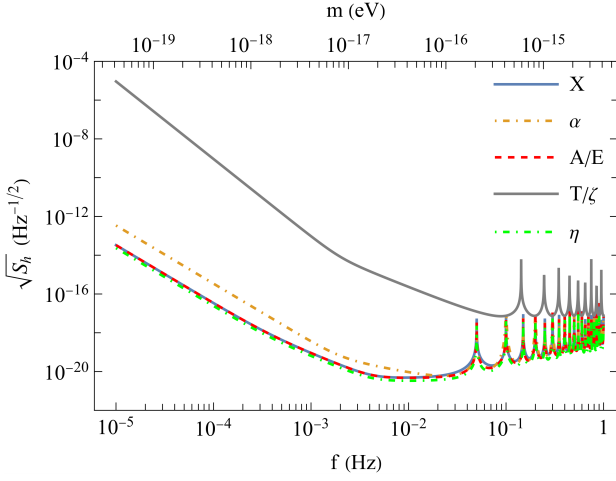


FIG. 4. The comparison between sensitivity curves of different channels for spin-2 ULDM.

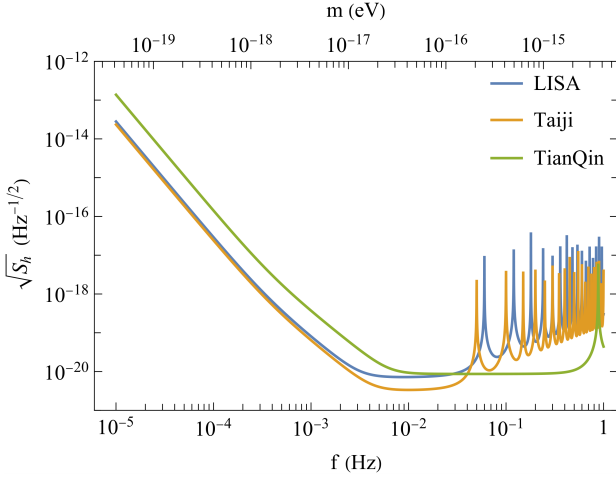


FIG. 5. The comparison between optimal sensitivity curves of different detectors for spin-2 ULDM.

tion, and the motion of the solar system should also be taken into consideration. Stochastic fluctuations of spin-2 ULDM are also important factors [38]. After careful consideration of these effects, the constraint for the coupling constant may be weakened. In the future, we would conduct a more comprehensive study on the detectability of spin-2 ULDM with space-based GWIs.

ACKNOWLEDGMENTS

This work is supported by the National Key Research and Development Program of China (Nos. 2023YFC2206200, 2020YFC2201502, 2021YFA0718304), the National Natural Science Foundation of China (No.12375059 and No.12235019) and the Fundamental Research Funds for the Central Universities (No. E2ET0209X2). We thank Yong Tang and Jiang-Chuan

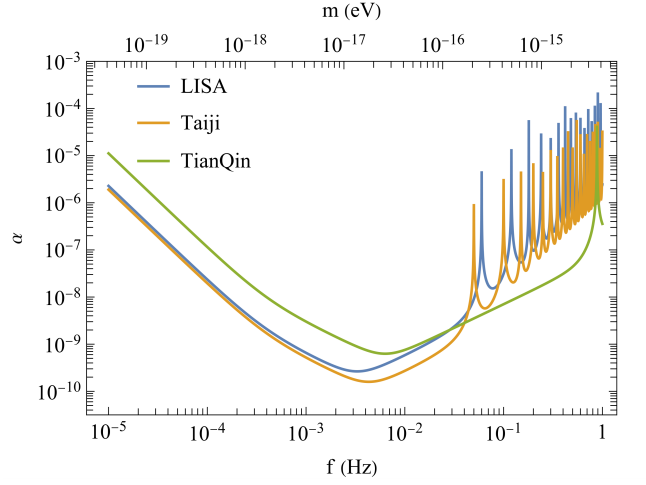


FIG. 6. The constraints on coupling parameter α for spin-2 ULDM. The observation time is set to be $T_{\text{obs}} = 1$ yr.

Yu for many helpful discussions.

Appendix A: Sagnac TDI combinations

In this section, we summarise the detector tensor and transfer functions in Sagnac TDI combinations.

1. Sagnac combinations

For Sagnac combination α , the signal

$$s_{\alpha}(t) = \frac{1}{3L} [\ell_{31}(t-3L) + \ell_{23}(t-2L) + \ell_{12}(t-L) - \ell_{21}(t-3L) - \ell_{32}(t-2L) - \ell_{13}(t-L)] = \mathbf{D}_{\alpha}^{ij}(\vec{v}) h_{ij}(t, \vec{x}_1). \quad (\text{A1})$$

The corresponding detector tensor is given by

$$\mathbf{D}_{\alpha}^{ij}(\vec{v}) = \frac{1}{6} [n_{21}^i n_{21}^j \mathcal{T}_{\alpha,21}(\vec{v} \cdot \hat{n}_{21}) + n_{32}^i n_{32}^j \mathcal{T}_{\alpha,32}(\vec{v} \cdot \hat{n}_{32}) + n_{13}^i n_{13}^j \mathcal{T}_{\alpha,13}(\vec{v} \cdot \hat{n}_{13})], \quad (\text{A2})$$

where the transfer functions are

$$\begin{aligned} \mathcal{T}_{\alpha,21}(\vec{v} \cdot \hat{n}_{21}) &= -\text{sinc}(\phi_m(1 + \vec{v} \cdot \hat{n}_{21})) e^{i\phi_m(-5 + \vec{v} \cdot \hat{n}_{21})} \\ &\quad + \text{sinc}(\phi_m(1 - \vec{v} \cdot \hat{n}_{21})) e^{i\phi_m(-1 + \vec{v} \cdot \hat{n}_{21})}, \\ \mathcal{T}_{\alpha,32}(\vec{v} \cdot \hat{n}_{32}) &= [-\text{sinc}(\phi_m(1 + \vec{v} \cdot \hat{n}_{32})) \\ &\quad + \text{sinc}(\phi_m(1 - \vec{v} \cdot \hat{n}_{32}))] e^{i\phi_m(-3 + \vec{v} \cdot (\hat{n}_{21} - \hat{n}_{13}))}, \\ \mathcal{T}_{\alpha,13}(\vec{v} \cdot \hat{n}_{13}) &= -\text{sinc}(\phi_m(1 + \vec{v} \cdot \hat{n}_{13})) e^{i\phi_m(-1 - \vec{v} \cdot \hat{n}_{13})} \\ &\quad + \text{sinc}(\phi_m(1 - \vec{v} \cdot \hat{n}_{13})) e^{i\phi_m(-5 - \vec{v} \cdot \hat{n}_{13})}. \end{aligned} \quad (\text{A3})$$

Note that the transfer functions for different arms here have distinct forms, which is due to our choice of

$h_{ij}(t, \vec{x}_1)$. The Sagnac combinations β and γ are cyclic permutations of Eq. (A1).

The comparison between spin-2 ULDM and GWs for Sagnac α combinations is depicted in Fig. 2. At low frequencies, the response of spin-2 ULDM is stronger than that of GWs. The low frequency limit of the response function for spin-2 ULDM is $\frac{2}{3}\pi^2 L^2 f^2$, and the ratio between spin-2 ULDM and GWs responses is still $\frac{5}{2}$. At high frequencies, the spin-2 ULDM exhibits different behavior compared to GWs. When the frequency is near odd multiples of $\frac{1}{2L}$, both response curves drop, with the response for spin-2 ULDM being lower due to its lower speed. When the frequency is near even multiples of $\frac{1}{2L}$, the response for spin-2 ULDM drops, while the response for GWs remains unaffected.

2. Fully symmetric Sagnac combination

The fully symmetric Sagnac combination ζ is given by

$$\begin{aligned} s_\zeta(t) &= \frac{1}{3L} [\ell_{21}(t-L) - \ell_{12}(t-L) + \ell_{13}(t-L) \\ &\quad - \ell_{31}(t-L) + \ell_{32}(t-L) - \ell_{23}(t-L)] \\ &= D_\zeta^{ij}(\vec{v}) h_{ij}(t, \vec{x}_1). \end{aligned} \quad (\text{A4})$$

The corresponding detector tensor is

$$\begin{aligned} D_\zeta^{ij}(\vec{v}) &= \frac{1}{6} [n_{21}^i n_{21}^j \mathcal{T}_{\zeta,21}(\vec{v} \cdot \hat{n}_{21}) + n_{32}^i n_{32}^j \mathcal{T}_{\zeta,32}(\vec{v} \cdot \hat{n}_{32}) \\ &\quad + n_{13}^i n_{13}^j \mathcal{T}_{\zeta,13}(\vec{v} \cdot \hat{n}_{13})], \end{aligned} \quad (\text{A5})$$

where the transfer functions are

$$\begin{aligned} \mathcal{T}_{\zeta,21}(\vec{v} \cdot \hat{n}_{21}) &= e^{i\phi_m(-1+\vec{v} \cdot \hat{n}_{21})} \\ &\quad \times [\text{sinc}(\phi_m(1+\vec{v} \cdot \hat{n}_{21})) - \text{sinc}(\phi_m(1-\vec{v} \cdot \hat{n}_{21}))], \\ \mathcal{T}_{\zeta,32}(\vec{v} \cdot \hat{n}_{32}) &= e^{i\phi_m(-1+\vec{v} \cdot (\hat{n}_{21}-\hat{n}_{13}))} \\ &\quad \times [\text{sinc}(\phi_m(1+\vec{v} \cdot \hat{n}_{32})) - \text{sinc}(\phi_m(1-\vec{v} \cdot \hat{n}_{32}))], \\ \mathcal{T}_{\zeta,13}(\vec{v} \cdot \hat{n}_{13}) &= e^{i\phi_m(-1-\vec{v} \cdot \hat{n}_{13})} \\ &\quad \times [\text{sinc}(\phi_m(1+\vec{v} \cdot \hat{n}_{13})) - \text{sinc}(\phi_m(1-\vec{v} \cdot \hat{n}_{13}))]. \end{aligned} \quad (\text{A6})$$

As shown in Fig. 2, it is obvious that the response of GWs greatly exceeds that of spin-2 GM for the ζ channel. This can be seen by Taylor expanding the response function for spin-2 ULDM with velocity v . The result is

$$\mathcal{R}_\zeta = \frac{(2 \sin \phi_m - 2 \phi_m \cos \phi_m)^2}{48 \phi_m^2} v^2 + \mathcal{O}(v^4), \quad (\text{A7})$$

which has no zeroth-order terms. Therefore, the response function is strongly suppressed by the velocity v .

Appendix B: AET channels

For AET channels [75], the signals are given by

$$s_A(t) = \frac{1}{\sqrt{2}} [s_Z(t) - s_X(t)] = D_A^{ij}(\vec{v}) h_{ij}(t, \vec{x}_1),$$

$$\begin{aligned} s_E(t) &= \frac{1}{\sqrt{6}} [s_X(t) - 2s_Y(t) + s_Z(t)] = D_E^{ij}(\vec{v}) h_{ij}(t, \vec{x}_1), \\ s_T(t) &= \frac{1}{\sqrt{3}} [s_X(t) + s_Y(t) + s_Z(t)] = D_T^{ij}(\vec{v}) h_{ij}(t, \vec{x}_1). \end{aligned} \quad (\text{B1})$$

The relating functions are calculated as follows. The detector tensor for A channel is given by

$$\begin{aligned} D_A^{ij}(\vec{v}) &= \frac{1}{4\sqrt{2}} [n_{21}^i n_{21}^j \mathcal{T}_{A,21}(\vec{v} \cdot \hat{n}_{21}) + n_{32}^i n_{32}^j \mathcal{T}_{A,32}(\vec{v} \cdot \hat{n}_{32}) \\ &\quad + n_{13}^i n_{13}^j \mathcal{T}_{A,13}(\vec{v} \cdot \hat{n}_{13})], \end{aligned} \quad (\text{B2})$$

where the transfer functions are

$$\begin{aligned} \mathcal{T}_{A,21}(\vec{v} \cdot \hat{n}_{21}) &= i \sin(2\phi_m) [\text{sinc}(\phi_m(1+\vec{v} \cdot \hat{n}_{21})) \\ &\quad + \text{sinc}(\phi_m(1-\vec{v} \cdot \hat{n}_{21}))] e^{i\phi_m(-5+\vec{v} \cdot \hat{n}_{21})}, \\ \mathcal{T}_{A,32}(\vec{v} \cdot \hat{n}_{32}) &= i \sin(2\phi_m) [\text{sinc}(\phi_m(1+\vec{v} \cdot \hat{n}_{32})) e^{i2\phi_m} \\ &\quad + \text{sinc}(\phi_m(1-\vec{v} \cdot \hat{n}_{32}))] e^{i\phi_m(-5+\vec{v} \cdot (\hat{n}_{21}-\hat{n}_{13}))}, \\ \mathcal{T}_{A,13}(\vec{v} \cdot \hat{n}_{13}) &= -2i \sin(2\phi_m) [\text{sinc}(\phi_m(1+\vec{v} \cdot \hat{n}_{13})) \\ &\quad + \text{sinc}(\phi_m(1-\vec{v} \cdot \hat{n}_{13}))] \cos(\phi_m) e^{i\phi_m(-4-\vec{v} \cdot \hat{n}_{13})}. \end{aligned} \quad (\text{B3})$$

The detector tensor for E channel is calculated as

$$\begin{aligned} D_E^{ij}(\vec{v}) &= \frac{1}{4\sqrt{6}} [n_{21}^i n_{21}^j \mathcal{T}_{E,21}(\vec{v} \cdot \hat{n}_{21}) + n_{32}^i n_{32}^j \mathcal{T}_{E,32}(\vec{v} \cdot \hat{n}_{32}) \\ &\quad + n_{13}^i n_{13}^j \mathcal{T}_{E,13}(\vec{v} \cdot \hat{n}_{13})], \end{aligned} \quad (\text{B4})$$

where the transfer functions are

$$\begin{aligned} \mathcal{T}_{E,21}(\vec{v} \cdot \hat{n}_{21}) &= -i [(1 + 2e^{i2\phi_m}) \text{sinc}(\phi_m(1+\vec{v} \cdot \hat{n}_{21})) \\ &\quad + (2 + e^{i2\phi_m}) \text{sinc}(\phi_m(1-\vec{v} \cdot \hat{n}_{21}))] \\ &\quad \times \sin(2\phi_m) e^{i\phi_m(-5+\vec{v} \cdot \hat{n}_{21})}, \\ \mathcal{T}_{E,32}(\vec{v} \cdot \hat{n}_{32}) &= i [(2 + e^{i2\phi_m}) \text{sinc}(\phi_m(1+\vec{v} \cdot \hat{n}_{32})) \\ &\quad + (1 + 2e^{i2\phi_m}) \text{sinc}(\phi_m(1-\vec{v} \cdot \hat{n}_{32}))] \\ &\quad \times \sin(2\phi_m) e^{i\phi_m(-5+\vec{v} \cdot (\hat{n}_{21}-\hat{n}_{13}))}, \\ \mathcal{T}_{E,13}(\vec{v} \cdot \hat{n}_{13}) &= -2 \sin(2\phi_m) \sin(\phi_m) e^{i\phi_m(-4-\vec{v} \cdot \hat{n}_{13})} \\ &\quad \times [\text{sinc}(\phi_m(1+\vec{v} \cdot \hat{n}_{13})) - \text{sinc}(\phi_m(1-\vec{v} \cdot \hat{n}_{13}))]. \end{aligned} \quad (\text{B5})$$

The detector tensor for T channel is calculated as

$$\begin{aligned} D_T^{ij}(\vec{v}) &= \frac{1}{2\sqrt{3}} [n_{21}^i n_{21}^j \mathcal{T}_{T,21}(\vec{v} \cdot \hat{n}_{21}) + n_{32}^i n_{32}^j \mathcal{T}_{T,32}(\vec{v} \cdot \hat{n}_{32}) \\ &\quad + n_{13}^i n_{13}^j \mathcal{T}_{T,13}(\vec{v} \cdot \hat{n}_{13})], \end{aligned} \quad (\text{B6})$$

where the transfer functions are

$$\begin{aligned} \mathcal{T}_{T,21}(\vec{v} \cdot \hat{n}_{21}) &= -\sin(2\phi_m) \sin(\phi_m) e^{i\phi_m(-4+\vec{v} \cdot \hat{n}_{21})} \\ &\quad \times [\text{sinc}(\phi_m(1+\vec{v} \cdot \hat{n}_{21})) - \text{sinc}(\phi_m(1-\vec{v} \cdot \hat{n}_{21}))], \\ \mathcal{T}_{T,32}(\vec{v} \cdot \hat{n}_{32}) &= -\sin(2\phi_m) \sin(\phi_m) e^{i\phi_m(-4+\vec{v} \cdot (\hat{n}_{21}-\hat{n}_{13}))} \\ &\quad \times [\text{sinc}(\phi_m(1+\vec{v} \cdot \hat{n}_{32})) - \text{sinc}(\phi_m(1-\vec{v} \cdot \hat{n}_{32}))], \end{aligned}$$

$$\begin{aligned} \mathcal{T}_{T,13}(\vec{v} \cdot \hat{n}_{13}) &= -\sin(2\phi_m) \sin(\phi_m) e^{i\phi_m(-4-\vec{v} \cdot \hat{n}_{13})} \\ &\times \left[\text{sinc}(\phi_m(1 + \vec{v} \cdot \hat{n}_{13})) - \text{sinc}(\phi_m(1 - \vec{v} \cdot \hat{n}_{13})) \right]. \end{aligned} \quad (\text{B7})$$

Note that although the T channel is fully symmetric for three arms. Since we choose $h_{ij}(t, \vec{x}_1)$ as the signal, similarly as in Sec. A 2, the transfer functions acquire their asymmetric forms.

After numerical calculation, the response functions for A channel and E channel are the same, which are shown in Fig. 2 together with the T channel. From Sec. A 2 and Fig. 2, we can see that ζ channel and T channel are

similar to each other, with the response of GWs being better than of spin-2 ULDM. In fact, these two channels are related by the following simple relation:

$$\mathcal{R}_T = 3 \sin^2(\pi f L) \sin^2(2\pi f L) \mathcal{R}_\zeta. \quad (\text{B8})$$

The reason for the weak response of spin-2 ULDM in T and ζ channel may be attributed to their symmetric features. This effect, combined with the low velocity of spin-2 ULDM, as discussed in Sec. A 2, results in insensitive performance of the response function.

-
- [1] B. P. Abbott *et al.* (LIGO Scientific, Virgo), Observation of Gravitational Waves from a Binary Black Hole Merger, *Phys. Rev. Lett.* **116**, 061102 (2016), [arXiv:1602.03837 \[gr-qc\]](#).
- [2] B. P. Abbott *et al.* (LIGO Scientific, Virgo), GW170817: Observation of Gravitational Waves from a Binary Neutron Star Inspiral, *Phys. Rev. Lett.* **119**, 161101 (2017), [arXiv:1710.05832 \[gr-qc\]](#).
- [3] G. Agazie *et al.* (NANOGrav), The NANOGrav 15 yr Data Set: Evidence for a Gravitational-wave Background, *Astrophys. J. Lett.* **951**, L8 (2023), [arXiv:2306.16213 \[astro-ph.HE\]](#).
- [4] J. Antoniadis *et al.* (EPTA, InPTA:), The second data release from the European Pulsar Timing Array - III. Search for gravitational wave signals, *Astron. Astrophys.* **678**, A50 (2023), [arXiv:2306.16214 \[astro-ph.HE\]](#).
- [5] D. J. Reardon *et al.*, Search for an Isotropic Gravitational-wave Background with the Parkes Pulsar Timing Array, *Astrophys. J. Lett.* **951**, L6 (2023), [arXiv:2306.16215 \[astro-ph.HE\]](#).
- [6] H. Xu *et al.*, Searching for the Nano-Hertz Stochastic Gravitational Wave Background with the Chinese Pulsar Timing Array Data Release I, *Res. Astron. Astrophys.* **23**, 075024 (2023), [arXiv:2306.16216 \[astro-ph.HE\]](#).
- [7] P. A. R. Ade *et al.* (BICEP, Keck), Improved Constraints on Primordial Gravitational Waves using Planck, WMAP, and BICEP/Keck Observations through the 2018 Observing Season, *Phys. Rev. Lett.* **127**, 151301 (2021), [arXiv:2110.00483 \[astro-ph.CO\]](#).
- [8] H. Li *et al.*, Probing Primordial Gravitational Waves: Ali CMB Polarization Telescope, *Natl. Sci. Rev.* **6**, 145 (2019), [arXiv:1710.03047 \[astro-ph.CO\]](#).
- [9] D. Wang, Primordial Gravitational Waves 2024, (2024), [arXiv:2407.02714 \[astro-ph.CO\]](#).
- [10] A. W. Adams and J. S. Bloom, Direct detection of dark matter with space-based laser interferometers, (2004), [arXiv:astro-ph/0405266](#).
- [11] E. D. Hall, R. X. Adhikari, V. V. Frolov, H. Müller, M. Pospelov, and R. X. Adhikari, Laser Interferometers as Dark Matter Detectors, *Phys. Rev. D* **98**, 083019 (2018), [arXiv:1605.01103 \[gr-qc\]](#).
- [12] C.-R. Chen and C. S. Nugroho, Detection prospects of dark matter in the Einstein Telescope, *Phys. Rev. D* **105**, 083001 (2022), [arXiv:2111.11014 \[hep-ph\]](#).
- [13] L. Heisenberg, D. Maibach, and D. Veske, Searching for topological dark matter in LIGO data, *Phys. Rev. D* **110**, 055037 (2024), [arXiv:2309.05093 \[gr-qc\]](#).
- [14] E. G. M. Ferreira, Ultra-light dark matter, *Astron. Astrophys. Rev.* **29**, 7 (2021), [arXiv:2005.03254 \[astro-ph.CO\]](#).
- [15] L. Hui, Wave Dark Matter, *Ann. Rev. Astron. Astrophys.* **59**, 247 (2021), [arXiv:2101.11735 \[astro-ph.CO\]](#).
- [16] M. Aghaie, G. Armando, A. Dondarini, and P. Pani, Bounds on ultralight dark matter from NANOGrav, *Phys. Rev. D* **109**, 103030 (2024), [arXiv:2308.04590 \[astro-ph.CO\]](#).
- [17] B. C. Bromley, P. Sandick, and B. Shams Es Haghi, Supermassive black hole binaries in ultralight dark matter, *Phys. Rev. D* **110**, 023517 (2024), [arXiv:2311.18013 \[astro-ph.GA\]](#).
- [18] S. D. B. Fell, L. Heisenberg, and D. Veske, Detecting fundamental vector fields with LISA, *Phys. Rev. D* **108**, 083010 (2023), [arXiv:2304.14129 \[gr-qc\]](#).
- [19] R. Brito, V. Cardoso, and P. Pani, Superradiance: New Frontiers in Black Hole Physics, *Lect. Notes Phys.* **906**, pp.1 (2015), [arXiv:1501.06570 \[gr-qc\]](#).
- [20] R. Brito, S. Ghosh, E. Barausse, E. Berti, V. Cardoso, I. Dvorkin, A. Klein, and P. Pani, Stochastic and resolvable gravitational waves from ultralight bosons, *Phys. Rev. Lett.* **119**, 131101 (2017), [arXiv:1706.05097 \[gr-qc\]](#).
- [21] R. Brito, S. Ghosh, E. Barausse, E. Berti, V. Cardoso, I. Dvorkin, A. Klein, and P. Pani, Gravitational wave searches for ultralight bosons with LIGO and LISA, *Phys. Rev. D* **96**, 064050 (2017), [arXiv:1706.06311 \[gr-qc\]](#).
- [22] M. Isi, L. Sun, R. Brito, and A. Melatos, Directed searches for gravitational waves from ultralight bosons, *Phys. Rev. D* **99**, 084042 (2019), [Erratum: *Phys. Rev. D* **102**, 049901 (2020)], [arXiv:1810.03812 \[gr-qc\]](#).
- [23] C. Yuan, R. Brito, and V. Cardoso, Probing ultralight dark matter with future ground-based gravitational-wave detectors, *Phys. Rev. D* **104**, 044011 (2021), [arXiv:2106.00021 \[gr-qc\]](#).
- [24] C. Yuan, Y. Jiang, and Q.-G. Huang, Constraints on an ultralight scalar boson from Advanced LIGO and Advanced Virgo's first three observing runs using the stochastic gravitational-wave background, *Phys. Rev. D* **106**, 023020 (2022), [arXiv:2204.03482 \[astro-ph.CO\]](#).
- [25] R.-Z. Guo, Y. Jiang, and Q.-G. Huang, Probing ultralight tensor dark matter with the stochastic gravitational-wave background from advanced LIGO and Virgo's first three observing runs, *JCAP* **04**, 053, [arXiv:2312.16435 \[astro-ph.CO\]](#).

- [26] A. Pierce, K. Riles, and Y. Zhao, Searching for Dark Photon Dark Matter with Gravitational Wave Detectors, *Phys. Rev. Lett.* **121**, 061102 (2018), [arXiv:1801.10161 \[hep-ph\]](#).
- [27] S. Morisaki and T. Suyama, Detectability of ultralight scalar field dark matter with gravitational-wave detectors, *Phys. Rev. D* **100**, 123512 (2019), [arXiv:1811.05003 \[hep-ph\]](#).
- [28] K. Nagano, T. Fujita, Y. Michimura, and I. Obata, Axion Dark Matter Search with Interferometric Gravitational Wave Detectors, *Phys. Rev. Lett.* **123**, 111301 (2019), [arXiv:1903.02017 \[hep-ph\]](#).
- [29] H. Grote and Y. V. Stadnik, Novel signatures of dark matter in laser-interferometric gravitational-wave detectors, *Phys. Rev. Res.* **1**, 033187 (2019), [arXiv:1906.06193 \[astro-ph.IM\]](#).
- [30] Y. Michimura, T. Fujita, S. Morisaki, H. Nakatsuka, and I. Obata, Ultralight vector dark matter search with auxiliary length channels of gravitational wave detectors, *Phys. Rev. D* **102**, 102001 (2020), [arXiv:2008.02482 \[hep-ph\]](#).
- [31] J. M. Armaleo, D. López Nacir, and F. R. Urban, Searching for spin-2 ULDM with gravitational waves interferometers, *JCAP* **04**, 053, [arXiv:2012.13997 \[astro-ph.CO\]](#).
- [32] K. Nagano, H. Nakatsuka, S. Morisaki, T. Fujita, Y. Michimura, and I. Obata, Axion dark matter search using arm cavity transmitted beams of gravitational wave detectors, *Phys. Rev. D* **104**, 062008 (2021), [arXiv:2106.06800 \[hep-ph\]](#).
- [33] A. L. Miller, F. Badaracco, and C. Palomba (LIGO Scientific, Virgo, KAGRA), Distinguishing between dark-matter interactions with gravitational-wave detectors, *Phys. Rev. D* **105**, 103035 (2022), [arXiv:2204.03814 \[astro-ph.IM\]](#).
- [34] E. Hall and N. Aggarwal, Advanced LIGO, LISA, and Cosmic Explorer as dark matter transducers, (2022), [arXiv:2210.17487 \[hep-ex\]](#).
- [35] M. A. Ismail, C. S. Nugroho, and H. T.-K. Wong, Exploring dark photons via a subfrequency laser search in gravitational wave detectors, *Phys. Rev. D* **107**, 082002 (2023), [arXiv:2211.13384 \[hep-ph\]](#).
- [36] H. Kim, Gravitational interaction of ultralight dark matter with interferometers, *JCAP* **12**, 018, [arXiv:2306.13348 \[hep-ph\]](#).
- [37] J.-C. Yu, Y.-H. Yao, Y. Tang, and Y.-L. Wu, Sensitivity of space-based gravitational-wave interferometers to ultralight bosonic fields and dark matter, *Phys. Rev. D* **108**, 083007 (2023), [arXiv:2307.09197 \[gr-qc\]](#).
- [38] Y.-H. Yao and Y. Tang, Probing Stochastic Ultralight Dark Matter with Space-based Gravitational-Wave Interferometers, (2024), [arXiv:2404.01494 \[hep-ph\]](#).
- [39] J.-C. Yu, Y. Cao, Y. Tang, and Y.-L. Wu, Detecting ultralight dark matter gravitationally with laser interferometers in space, *Phys. Rev. D* **110**, 023025 (2024), [arXiv:2404.04333 \[hep-ph\]](#).
- [40] H.-K. Guo, K. Riles, F.-W. Yang, and Y. Zhao, Searching for Dark Photon Dark Matter in LIGO O1 Data, *Commun. Phys.* **2**, 155 (2019), [arXiv:1905.04316 \[hep-ph\]](#).
- [41] A. L. Miller *et al.*, Probing new light gauge bosons with gravitational-wave interferometers using an adapted semicoherent method, *Phys. Rev. D* **103**, 103002 (2021), [arXiv:2010.01925 \[astro-ph.IM\]](#).
- [42] S. Morisaki, T. Fujita, Y. Michimura, H. Nakatsuka, and I. Obata, Improved sensitivity of interferometric gravitational wave detectors to ultralight vector dark matter from the finite light-traveling time, *Phys. Rev. D* **103**, L051702 (2021), [arXiv:2011.03589 \[hep-ph\]](#).
- [43] S. M. Vermeulen *et al.*, Direct limits for scalar field dark matter from a gravitational-wave detector [10.1038/s41586-021-04031-y](#) (2021), [arXiv:2103.03783 \[gr-qc\]](#).
- [44] R. Abbott *et al.* (LIGO Scientific, KAGRA, Virgo), Constraints on dark photon dark matter using data from LIGO's and Virgo's third observing run, *Phys. Rev. D* **105**, 063030 (2022), [Erratum: *Phys. Rev. D* **109**, 089902 (2024)], [arXiv:2105.13085 \[astro-ph.CO\]](#).
- [45] L. Aiello, J. W. Richardson, S. M. Vermeulen, H. Grote, C. Hogan, O. Kwon, and C. Stoughton, Constraints on Scalar Field Dark Matter from Colocated Michelson Interferometers, *Phys. Rev. Lett.* **128**, 121101 (2022), [arXiv:2108.04746 \[gr-qc\]](#).
- [46] A. L. Miller and L. Mendes, First search for ultralight dark matter with a space-based gravitational-wave antenna: LISA Pathfinder, *Phys. Rev. D* **107**, 063015 (2023), [arXiv:2301.08736 \[gr-qc\]](#).
- [47] K. Fukusumi, S. Morisaki, and T. Suyama, Upper limit on scalar field dark matter from LIGO-Virgo third observation run, *Phys. Rev. D* **108**, 095054 (2023), [arXiv:2303.13088 \[hep-ph\]](#).
- [48] J. Frerick, J. Jaeckel, F. Kahlhoefer, and K. Schmidt-Hoberg, Riding the dark matter wave: Novel limits on general dark photons from LISA Pathfinder, *Phys. Lett. B* **848**, 138328 (2024), [arXiv:2310.06017 \[hep-ph\]](#).
- [49] Y. Manita, H. Takeda, K. Aoki, T. Fujita, and S. Mukohyama, Exploring the spin of ultralight dark matter with gravitational wave detectors, *Phys. Rev. D* **109**, 095012 (2024), [arXiv:2310.10646 \[hep-ph\]](#).
- [50] A. S. Göttel, A. Ejlli, K. Karan, S. M. Vermeulen, L. Aiello, V. Raymond, and H. Grote, Searching for Scalar Field Dark Matter with LIGO, *Phys. Rev. Lett.* **133**, 101001 (2024), [arXiv:2401.18076 \[astro-ph.CO\]](#).
- [51] A. G. Abac *et al.* (KAGRA, LIGO Scientific, VIRGO), Ultralight vector dark matter search using data from the KAGRA O3GK run, *Phys. Rev. D* **110**, 042001 (2024), [arXiv:2403.03004 \[astro-ph.CO\]](#).
- [52] Q. L. Nguyen and A. L. Miller, Dark Matter and its Effect on Gravitational Wave Signal, *PoS EPS-HEP2023*, 132 (2024).
- [53] Y. Xie, A. K.-W. Chung, T. P. Sotiriou, and N. Yunes, Bayesian search of massive scalar fields from LIGO-Virgo-KAGRA binaries, (2024), [arXiv:2410.14801 \[gr-qc\]](#).
- [54] J. M. Armaleo, D. López Nacir, and F. R. Urban, Pulsar timing array constraints on spin-2 ULDM, *JCAP* **09**, 031, [arXiv:2005.03731 \[astro-ph.CO\]](#).
- [55] S. Sun, X.-Y. Yang, and Y.-L. Zhang, Pulsar timing residual induced by wideband ultralight dark matter with spin 0,1,2, *Phys. Rev. D* **106**, 066006 (2022), [arXiv:2112.15593 \[astro-ph.CO\]](#).
- [56] C. Unal, F. R. Urban, and E. D. Kovetz, Probing ultralight scalar, vector and tensor dark matter with pulsar timing arrays, *Phys. Lett. B* **855**, 138830 (2024), [arXiv:2209.02741 \[astro-ph.CO\]](#).
- [57] Y.-M. Wu, Z.-C. Chen, and Q.-G. Huang, Pulsar timing residual induced by ultralight tensor dark matter, *JCAP* **09**, 021, [arXiv:2305.08091 \[hep-ph\]](#).
- [58] P. Amaro-Seoane *et al.* (LISA), Laser Interferometer Space Antenna, (2017), [arXiv:1702.00786 \[astro-ph.IM\]](#).

- [59] W.-R. Hu and Y.-L. Wu, The Taiji Program in Space for gravitational wave physics and the nature of gravity, *Natl. Sci. Rev.* **4**, 685 (2017).
- [60] J. Luo *et al.* (TianQin), TianQin: a space-borne gravitational wave detector, *Class. Quant. Grav.* **33**, 035010 (2016), [arXiv:1512.02076 \[astro-ph.IM\]](#).
- [61] M. Tinto and S. V. Dhurandhar, Time-Delay Interferometry, *Living Rev. Rel.* **8**, 4 (2005), [arXiv:gr-qc/0409034](#).
- [62] S. L. Dubovsky, P. G. Tinyakov, and I. I. Tkachev, Massive graviton as a testable cold dark matter candidate, *Phys. Rev. Lett.* **94**, 181102 (2005), [arXiv:hep-th/0411158](#).
- [63] S. F. Hassan and R. A. Rosen, Bimetric Gravity from Ghost-free Massive Gravity, *JHEP* **02**, 126, [arXiv:1109.3515 \[hep-th\]](#).
- [64] K. Aoki and S. Mukohyama, Massive gravitons as dark matter and gravitational waves, *Phys. Rev. D* **94**, 024001 (2016), [arXiv:1604.06704 \[hep-th\]](#).
- [65] E. Babichev, L. Marzola, M. Raidal, A. Schmidt-May, F. Urban, H. Veermäe, and M. von Strauss, Bigravitational origin of dark matter, *Phys. Rev. D* **94**, 084055 (2016), [arXiv:1604.08564 \[hep-ph\]](#).
- [66] E. Babichev, L. Marzola, M. Raidal, A. Schmidt-May, F. Urban, H. Veermäe, and M. von Strauss, Heavy spin-2 Dark Matter, *JCAP* **09**, 016, [arXiv:1607.03497 \[hep-th\]](#).
- [67] K. Aoki and K.-i. Maeda, Condensate of Massive Graviton and Dark Matter, *Phys. Rev. D* **97**, 044002 (2018), [arXiv:1707.05003 \[hep-th\]](#).
- [68] L. Marzola, M. Raidal, and F. R. Urban, Oscillating Spin-2 Dark Matter, *Phys. Rev. D* **97**, 024010 (2018), [arXiv:1708.04253 \[hep-ph\]](#).
- [69] Z.-Q. Xia, T.-P. Tang, X. Huang, Q. Yuan, and Y.-Z. Fan, Constraining ultralight dark matter using the Fermi-LAT pulsar timing array, *Phys. Rev. D* **107**, L121302 (2023), [arXiv:2303.17545 \[astro-ph.HE\]](#).
- [70] R.-G. Cai, J.-R. Zhang, and Y.-L. Zhang, Angular correlation and deformed Hellings-Downs curve from spin-2 ultralight dark matter, *Phys. Rev. D* **110**, 044052 (2024), [arXiv:2402.03984 \[gr-qc\]](#).
- [71] N. J. Cornish, Detecting a stochastic gravitational wave background with the Laser Interferometer Space Antenna, *Phys. Rev. D* **65**, 022004 (2002), [arXiv:gr-qc/0106058](#).
- [72] T. Robson, N. J. Cornish, and C. Liu, The construction and use of LISA sensitivity curves, *Class. Quant. Grav.* **36**, 105011 (2019), [arXiv:1803.01944 \[astro-ph.HE\]](#).
- [73] V. S. H. Lee and K. M. Zurek, Proper Time Observables of General Gravitational Perturbations in Laser Interferometry-based Gravitational Wave Detectors, (2024), [arXiv:2408.03363 \[hep-ph\]](#).
- [74] M. Maggiore, *Gravitational Waves. Vol. 2: Astrophysics and Cosmology* (Oxford University Press, 2018).
- [75] T. A. Prince, M. Tinto, S. L. Larson, and J. W. Armstrong, The LISA optimal sensitivity, *Phys. Rev. D* **66**, 122002 (2002), [arXiv:gr-qc/0209039](#).